EPJ D
Atomic, Molecular, Optical and Plasma Physics
EPJ.org
your physics journal

Eur. Phys. J. D (2015) 69: 148 DOI: 10.1140/epjd/e2015-60071-2

Circular polarization of the Lyman-α_1 line radiation emitted by longitudinally-polarized electron impact excitation: effects of Breit interaction and radiation multipoles

Zhan-Bin Chen and Jiao-Long Zeng

edp sciences
Società Italiana di Fisica
Springer

Eur. Phys. J. D (2015) 69: 148
DOI: 10.1140/epjd/e2015-60071-2

THE EUROPEAN PHYSICAL JOURNAL D

Regular Article

Circular polarization of the Lyman-α_1 line radiation emitted by longitudinally-polarized electron impact excitation: effects of Breit interaction and radiation multipoles

Zhan-Bin Chen[a] and Jiao-Long Zeng[b]

College of Science, National University of Defense Technology, Changsha, Hunan 410073, P.R. China

Received 4 February 2015 / Received in final form 23 March 2015
Published online 4 June 2015 –

Abstract. Detailed calculations are carried out for the longitudinally-polarized electron impact excitation cross sections from the ground state $1s_{1/2}$ to the individual magnetic sublevels of the excited state $2p_{3/2}$ of highly charged H-like ions using a fully relativistic distorted-wave method. The influence of the Breit interaction and radiation multipoles on the circular polarization of X-ray radiation are investigated systematically. Our results show that the Breit interaction, as the dominant correction to the Coulomb interaction, may lead to a considerable change in the magnetic sublevels cross sections and circular polarizations of Lyman-α_1 ($2p_{3/2} \rightarrow 1s_{1/2}$) line radiation with a more pronounced effect at higher incident energies and/or atomic numbers. Moreover, the interference between the electric dipole ($E1$) decay and the magnetic quadrupole ($M2$) decay may significantly alter the circular polarizations of the emitted X-rays. The circular polarizations of the Lyman-α_1 line are exhibit a different behavior than the linear polarizations for the same transition line regarding the radiative electron capture [Weber et al., Phys. Rev. Lett. **105**, 243002 (2010)], radiative recombination [Bettadj et al., J. Phys. B **47**, 105205 (2014)], and electron-impact excitation processes [Chen et al., Phys. Rev. A. **90**, 012703 (2014)].

1 Introduction

Recent advances in the production and storage of highly charged ions have opened up new opportunities to explore electron-atom/ions collisions [1]. Investigation of electron impact excitation (EIE) collision process plays an important role in understanding the electron correlation, quantum electrodynamic (QED), and hyperfine interaction effects. Apart from its fundamental importance, EIE is responsible for the vast majority of X-ray radiation produced in kinds of plasmas [2]. In the past, the studies have mainly dealt with the total cross sections and rate coefficients. Much of today's interest, in contrast, is focused on the polarization properties of X-ray emission [1,3–10]. From the detailed analysis of the polarization, valuable information can be obtained about both the magnetic sublevels population of the excited states and the dynamical process. These properties have become indispensable tools for the diagnosis of plasma state and the analysis of complex spectra formation mechanism [4–13].

In recent years, the studies of the Breit interaction (BI) are of great interest in a variety of fundamental processes, especially for highly charged ions. Theorists have employed the BI in order to provide more accurate polarization data. For example, a comparison was made in reference [14] for the degree of linear polarization of the Lyman-α_1 ($2p_{3/2} \rightarrow 1s_{1/2}$) line for H-like ions following EIE process using the relativistic convergent close-coupling method. The results indicated that the BI is important to resolve the discrepancy between theory and experiments. Fontes et al. [15] studied the collision strengths of He-like ions following EIE using a fully relativistic distorted-wave (RDW) method. They pointed out that the effect of the BI is very significant for highly charged Xe^{52+} ions and is even non-negligible for low-Z Fe^{24+} ions. Wu et al. [16] showed that the BI makes the linear polarization of Be-like ions decrease, which character becomes larger as the incident electron energy and/or atomic number increases. There are also many other studies of the BI in other dynamical processes, such as dielectronic recombination (DR) [17–19], electron-impact ionization (EII) [20,21] and so on. On the other hand, for highly charged ions, multipole-mixing effects are of also great important in the polarization properties of X-ray emission. For example, Surzhykov et al. [3] investigated the polarization of the Lyman-α_1 line following the radiative recombination (RR) of bare, high-Z ions. They found that the $E1$-$M2$ interference may remarkably modify the angular distribution of the linear polarization. Matula et al. [1] investigated the angular correlations between the photons emitted in the DR of H-like U^{91+} ions. They found that the higher multipole components can notably

[a] e-mail: chenzb008@qq.com
[b] e-mail: jlzeng@nudt.edu.cn

modify the angular properties. Fritzsche et al. [22] investigated the multipole mixing effects on the radiative decay of the doubly excited resonances of He-like U^{90+} ions, following the K-LL DR of H-like U^{91+} ions. They found that the interference between the multipole components can either decrease or enhance the anisotropy of individual fine-structure transitions, and that this effect can be as large as a factor of 6. We [23] have studied the linear polarization properties of highly charged H-like and He-like ions following EIE. Results show that the $E1$-$M2$ interference effects depend on the atomic number and/or the incident electron energy.

Until the present, however, most studies have dealt with the linear polarization of X-ray radiation [22–35]. In contrast, fewer publications have reported the circular polarization properties of X-ray radiation, due to the fact that the measurement of the circular polarization of (hard) X-rays is a very challenging task. For example, for the Compton scattering of magnetized materials, the measurement of circular polarization is limited, both in precision and in the requirements for the X-ray intensity and energy [36]. As is well known, excitation of ions by collisions with a polarized electron beam will leads to a different population for the different magnetic sublevels of the final state [10,37–39]. The X-ray radiation in the decay of these sublevels will exhibits both linear and circular polarization. Some years ago, Inal et al. [38] investigated the circular polarization properties of X-ray emission of He-like Sc^{19+} ions. They show that hyperfine interaction effect has a more dominant effect in reducing the circular polarization near the excitation threshold. Later, the inner-shell ionization effect and relativistic effect on the circular polarization were also reported [10,39]. For the high-Z elements, some higher order effects can be probed more effectively as the innermost electrons are exposed to strong nuclear fields. However, to our knowledge, there have been no previous results for the multipole effects on the circular polarization properties of X-ray radiation in the high-Z domain. In particular, recent experiment [22] showed that the $E1$-$M2$ interference effects can reduce the linear polarization of Lyman-α_1 line radiation of H-like U^{91+} ions by about 15%. Therefore, a similar effect should also be expected for the circular polarization of radiation emitted by the longitudinally polarized EIE.

In the present work, the cross sections and the circular polarization properties of the Lyman-α_1 line X-ray radiation for highly charged H-like Fe^{25+}, Xe^{53+}, Dy^{65+}, and U^{91+} ions after impact excitation by the longitudinally-polarized electron beam are calculated using a fully RDW method [4,16,23]. The effects of the BI and the $E1$-$M2$ interference on the cross sections and the degree of circular polarizations of subsequent X-ray radiation are discussed details. The paper is organized as follows. In Section 2 the method and computation are briefly outlined. In Section 3 we present a systematic study of the BI and multipole effects, separately and combined, on the circular polarization of Lyman-α_1 line X-ray emission along an isoelectronic sequence and as a function of the incident energy. Finally, a few conclusions are drawn in Section 4.

2 Theoretical method

2.1 Calculations of the cross sections

In this study, for the atomic structure part of the calculations we used the atomic structure code GRASP92 [40]. For the continuum electron wave functions part of the calculations we used the component COWF of the RATIP package [16,27,41,42]. In the RDW method [4,16,23], the quantization axis (z axis) is taken along the incident electron beam, so $m_{l_i} = 0$ (the z axis component of the incident electron orbital angular momentum). The subscript $i\,(f)$ refers to the initial (final) state. We assume that the direction of the final scattered electron remains unobserved. Then, the general formula of the impact excitation cross section for the target atom/ion from $\beta_i J_i M_i$ to $\beta_f J_f M_f$ by the longitudinally-polarized electron beam can be given by improving the formula [37–39]

$$\begin{aligned}\sigma_{\varepsilon_i}(\beta_i J_i M_i - \beta_f J_f M_f) &= \frac{2\pi a_0^2}{k_i^2} \\ &\times \sum_{l_i,l_i',j_i,j_i',l_f,j_f,m_f,m_{s_i}} \sum_{J,J',M} (i)^{l_i - l_i'}[(2l_i+1)(2l_i'+1)]^{1/2} \\ &\times \exp[i(\delta_{\kappa_i} - \delta_{\kappa_i'})] C(l_i \frac{1}{2} m_{l_i} m_{s_i}; j_i m_i) \\ &\times C(l_i' \frac{1}{2} m_{l_i'} m_{s_i}; j_i' m_i) C(J_i j_i M_i m_i; JM) \\ &\times C(J_i j_i' M_i m_i; J' M) C(J_f j_f M_f m_f; JM) \\ &\times C(J_f j_f M_f m_f; J' M) R(\gamma_i, \gamma_f) R(\gamma_i', \gamma_f'). \end{aligned} \quad (1)$$

Here ε_i and a_0 is the incident energy and Bohr radius, respectively. C's are the Clebsch-Gordan coefficients. δ_{κ_i} is the phase factor for the continuum electron. κ is the relativistic quantum number.

$$\gamma_i = \varepsilon_i l_i j_i \beta_i J_i JM;\ \gamma_f = \varepsilon_f l_f j_f \beta_f J_f JM, \quad (2)$$

in which J and M are the quantum numbers corresponding to the total (target plus free electron) angular momentum and its z component, respectively. For the incident electron, j_i and m_i are the quantum numbers corresponding to the total angular momentum and its z component, respectively. l_i and m_{l_i} are the quantum numbers corresponding to the orbital angular momentum and its z component, respectively. k_i is the relativistic wave number. β represents other quantum numbers required to specify the initial and final states of the target ion in addition to its total angular momentum J and its z component M.

The collision matrix element $R(\gamma_i, \gamma_f)$ can be written as [23,27]

$$R(\gamma_i, \gamma_f) = \langle \Psi_{\gamma_f} | \sum_{p,q,p<q}^{N+1} (V_{Coul} + V_{Breit}) | \Psi_{\gamma_i} \rangle, \quad (3)$$

in which $\Psi_{\gamma_i}(\Psi_{\gamma_f})$ is the wave function for the initial (final) state of the impact system, respectively. V_{Breit} (V_{Coul}) is

the Breit (Coulomb) operator, respectively [40].

$$V_{Breit} = -\frac{\alpha_p \cdot \alpha_q}{r_{pq}} \cos(\omega_{pq} r_{pq}) + (\alpha_p \cdot \nabla_p)(\alpha_q \cdot \nabla_q) \frac{\cos(\omega_{pq} r_{pq}) - 1}{\omega_{pq}^2 r_{pq}}, \quad (4)$$

where ω_{pq} is the angular frequency of the exchanged virtual photon. α_p and α_q are the Dirac matrices. The collision strength $\Omega_{if}(\varepsilon_i)$ is given by:

$$\Omega_{if}(\varepsilon_i) = \frac{k_i^2 g_i}{\pi a_0^2} \sigma_{if}(\varepsilon_i) \quad (5)$$

where g_i is the statistical weight of the initial level.

2.2 Calculations of the circular polarizations

The circular polarization of X-ray radiation is defined as [37–39]

$$P_c = \frac{I_{\sigma^+} - I_{\sigma^-}}{I_{\sigma^+} + I_{\sigma^-}}, \quad (6)$$

where I_{σ^+} (I_{σ^-}) is the intensity of left (right) handed circularly polarized radiation, respectively. For an electric dipole Lyman-α_1 ($2p_{3/2} \rightarrow 1s_{1/2}$) radiation line, the angular distribution of the circular polarization $P_c(\theta)$ is given by [37]

$$P_c(\theta) = \frac{f1}{f2}, \quad (7)$$

where

$$f1 = \sum_{M_{J'}} N_{M_{J'}} (-1)^{M_{J'}+J} \sum_{X odd} (2X+1) \begin{pmatrix} 1 & 1 & X \\ 1 & -1 & 0 \end{pmatrix} \times \begin{pmatrix} X & J & J \\ 0 & -M_J & M_J \end{pmatrix} \begin{Bmatrix} X & J & J \\ J' & 1 & 1 \end{Bmatrix} P_X(\cos\theta) \quad (8)$$

and

$$f2 = \sum_{M_{J'}} N_{M_{J'}} (-1)^{M_{J'}+J} \sum_{X even} (2X+1) \begin{pmatrix} 1 & 1 & X \\ 1 & -1 & 0 \end{pmatrix} \times \begin{pmatrix} X & J & J \\ 0 & -M_J & M_J \end{pmatrix} \begin{Bmatrix} X & J & J \\ J' & 1 & 1 \end{Bmatrix} P_X(\cos\theta) \quad (9)$$

where $N_{M_{J'}}$ are the populations of magnetic sublevels for the final states (J to J' decay). $0 \le X \le 2$, $P_X(\cos\theta)$ are Legendre polynomials.

2.3 Calculations of the E1-M2 interference

To consider the $E1$-$M2$ interference, a theory of the circular polarization of X-ray radiation in the transition involving two different electromagnetic multipoles was developed by Inal et al. [38]. In the present work, for the $\beta_f J_f$ to $\beta_i J_i$ (J to J') decay allowed by both El and $M2$ transitions, the maximum degree of circular polarization $P_c(\theta = 0)$ (θ is the angle between the incident electron beam and the direction of observation of the emitted radiation) can be expressed in terms of the populations N_{M_J} or σ_{M_J} of the $\beta J M_J$ magnetic sublevels by [37–39]

$$P_c(\theta = 0) = \frac{N_{E1} + N_{M2} + N_{Int}}{D_{E1} + D_{M2} + D_{Int}}. \quad (10)$$

Here, the first, second, and third term is the El transition, the $M2$ transition and the interference term, respectively. These terms are given by [38]

$$N_{E1} = 3\sqrt{\frac{3}{2}}(2J+1) \begin{Bmatrix} 1 & 1 & 1 \\ J & J & J' \end{Bmatrix} \times A_{E1} \times \sum_{M_J} N_{M_J} (-1)^{M_J+J'} \begin{pmatrix} 1 & J & J \\ 0 & -M_J & M_J \end{pmatrix} \quad (11)$$

$$D_{E1} = A_{E1} \left[\sum_{M_J} N_{M_J} (-1)^{2J+1} + \sqrt{\frac{15}{2}}(2J+1) \times \begin{Bmatrix} 1 & 1 & 2 \\ J & J & J' \end{Bmatrix} \sum_{M_J} N_{M_J} (-1)^{M_J+J'} \begin{pmatrix} 2 & J & J \\ 0 & -M_J & M_J \end{pmatrix} \right] \quad (12)$$

$$N_{M2} = 5(2J+1) A_{M2} \sum_{M_J} N_{M_J} (-1)^{M_J+J'} \times \sum_{K=1,3} (2K+1) \times \begin{pmatrix} 2 & 2 & K \\ 1 & -1 & 0 \end{pmatrix} \begin{Bmatrix} 2 & 2 & K \\ J & J & J' \end{Bmatrix} \begin{pmatrix} K & J & J \\ 0 & -M_J & M_J \end{pmatrix} \quad (13)$$

$$D_{M2} = A_{M2} \left[\sum_{M_J} N_{M_J} (-1)^{2J+1} + 5(2J+1) \times \sum_{M_J} N_{M_J} (-1)^{M_J+J'} \times \sum_{K=2,4} (2K+1) \times \begin{pmatrix} 2 & 2 & K \\ 1 & -1 & 0 \end{pmatrix} \begin{Bmatrix} 2 & 2 & K \\ J & J & J' \end{Bmatrix} \begin{pmatrix} K & J & J \\ 0 & -M_J & M_J \end{pmatrix} \right] \quad (14)$$

$$N_{Int} = 5\sqrt{6}(2J+1) \begin{Bmatrix} 1 & 2 & 2 \\ J & J & J' \end{Bmatrix} \sqrt{A_{E1} A_{M2}} \times \sum_{M_J} N_{M_J} (-1)^{M_J+J'} \times \begin{pmatrix} 2 & J & J \\ 0 & -M_J & M_J \end{pmatrix} \quad (15)$$

$$D_{Int} = -2\sqrt{15}(2J+1) \sqrt{A_{E1} A_{M2}} \sum_{M_J} N_{M_J} (-1)^{M_J+J'} \times \sum_{K=1,3} (2K+1) \begin{pmatrix} 1 & 2 & K \\ 1 & -1 & 0 \end{pmatrix} \begin{Bmatrix} 1 & 2 & K \\ J & J & J' \end{Bmatrix} \times \begin{pmatrix} K & J & J \\ 0 & -M_J & M_J \end{pmatrix} \quad (16)$$

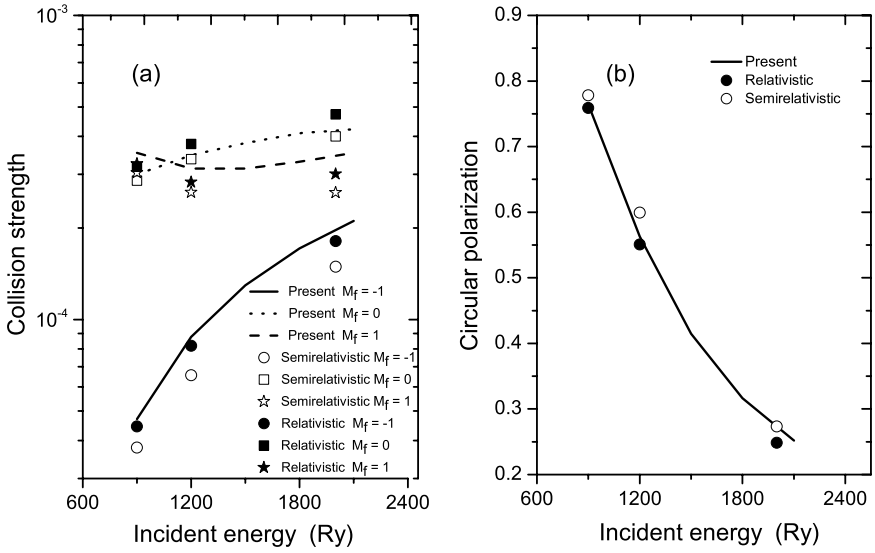

Fig. 1. Comparison of the (a) collision strength and (b) circular polarization $P_c(\theta = 0)$ of the $1s2p_{1/2}(J = 1) \rightarrow 1s^2\,(J = 0)$ transition line of He-like Fe^{24+} ions between the present calculated results and the existing theoretical results [37].

Table 1. Comparison of collision strengths for excitation from the ground level to specific magnetic sublevels of He-like Xe^{52+} ions by unpolarized electron for various impact energies. In each case, the upper entries are the present results, the second entries are the fully relativistic results given by Fontes et al. [15]. Here C + B and C represent the values with and without inclusion of BI, respectively. R[n] means $R \times 10^n$.

		3000 Ry		6000 Ry		10 000 Ry	
Excited state	M_f	C	C + B	C	C + B	C	C + B
$1s2s_{1/2}\,(J = 1)$	0	2.402[−5]	2.669[−5]	9.845[−6]	1.340[−5]	4.531[−6]	8.325[−6]
		2.425[−5]	2.713[−5]	9.917[−6]	1.382[−5]	4.559[−6]	8.345[−6]
	1	2.417[−5]	2.789[−5]	9.936[−6]	1.448[−5]	4.587[−6]	9.763[−6]
		2.428[−5]	2.791[−5]	9.969[−6]	1.478[−5]	4.612[−6]	9.886[−6]
	Total	7.236[−5]	8.127[−5]	2.972[−5]	4.236[−5]	1.370[−5]	2.785[−5]
		7.280[−5]	8.296[−5]	2.986[−5]	4.339[−5]	1.378[−5]	2.812[−5]
$1s2p_{1/2}\,(J = 1)$	Total	3.342[−4]	3.465[−4]	5.999[−4]	5.913[−4]	9.236[−4]	9.361[−4]
		3.400[−4]	3.517[−4]	6.056[−4]	6.047[−4]	9.410[−4]	9.579[−4]
$1s2p_{3/2}\,(J = 2)$	Total	1.473[−4]	1.717[−4]	4.275[−5]	6.160[−5]	1.552[−5]	3.289[−5]
		1.507[−4]	1.752[−4]	4.345[−5]	6.304[−5]	1.568[−5]	3.307[−5]

where A_{E1} (A_{M2}) is the pure $E1$ ($M2$) transition probability.

3 Calculations and discussions

3.1 Comparisons of collision strength and circular polarization

In order to check the accuracy of the present calculation, in Figure 1a, we display the collision strengths for the $1s^2(J = 0) \rightarrow 1s2p_{1/2}(J = 1)$ excitation of He-like Fe^{24+} ions by the longitudinally-polarized electrons. A slight discrepancy between our results and the theoretical predictions of Inal et al. [37] in the figure, which we attribute to the fact that the calculations in reference [37] do not include the BI in their scattering matrix elements. Figure 1b shows that the comparison of our circular polarization $P_c(\theta = 0)$ of subsequent X-ray emission of He-like Fe^{24+} ions results with that of reference [37] are in excellent agreement.

To further illustrate the accuracy of the present calculation for the high-Z ions, Table 1 gives the calculated collision strengths for unpolarized electron excitation of He-like Xe^{52+} ions from the ground level to specific magnetic sublevels for various impact energies, along with the available theoretical results [15]. From the table we can found that although our calculated collision strengths are a little smaller than those of Fontes et al. [15], the agreement of the different calculations is good. The maximal difference between the present results and the theoretical predictions of Fontes et al. [15] is within 3%. From the table we can also found that the effect of the BI on the

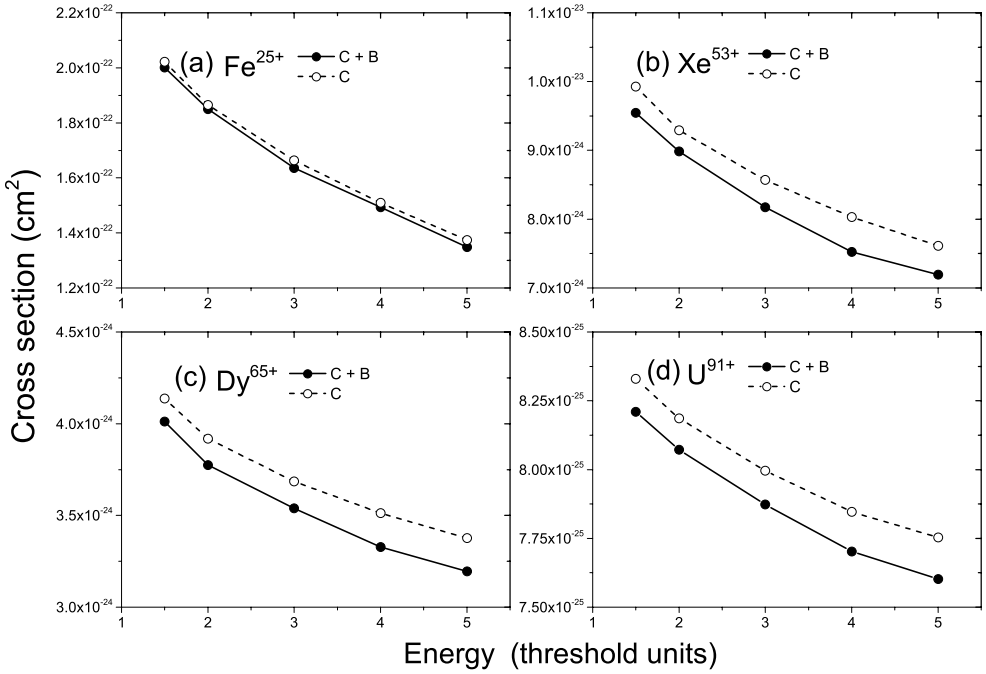

Fig. 2. Total cross section for longitudinally-polarized EIE from the ground state to the excited state $2p_{3/2}$ of H-like Fe^{25+}, Xe^{53+}, Dy^{65+}, and U^{91+} ions as functions of incident energy in threshold units. C + B and C represent the values with and without inclusion of BI, respectively.

collision strengths is quite different for different magnetic sublevels and incident energies. The BI has a fairly moderate effect near the threshold, while the effect becomes large for high incident energies.

3.2 BI effects on the cross sections

Figure 2 shows the total cross sections for direct excitation from the ground state $1s_{1/2}$ into the excited state $2p_{3/2}$ for unpolarized highly charged H-like Fe^{25+}, Xe^{53+}, Dy^{65+}, and U^{91+} ions as functions of incident longitudinally-polarized electron energy (threshold units). The threshold energies for these elements are 6977, 31334, 48139, and 118 873 eV, respectively. Here C + B and C represent the values with and without inclusion of BI, respectively. As shown in Figure 2, the cross sections both with and without the BI included decrease monotonically with increasing incident energy; they decrease rapidly/slowy within a lower/higher energy region. The BI has the effect of reducing the total cross sections at all energies and this becomes more significant at higher incident energy and for higher atomic numbers.

Figure 3 shows the $M_f = -1/2$ and $-3/2$ magnetic sublevels cross sections for direct excitation from the ground state $1s_{1/2}$ into the excited state $2p_{3/2}$ of highly charged H-like Fe^{25+}, Xe^{53+}, Dy^{65+}, and U^{91+} ions as functions of incident longitudinally-polarized electron energy. It can be found that the $M_f = -1/2$ sublevel is preferentially populated relative to the $M_f = -3/2$ sublevel in all the H-like ions and at all incident energies. As expected, for the low-Z H-like Fe^{25+} ions, differences between the cross sections with and without BI are very small. They do not exceed 10% for both the $M_f = -1/2$ and $-3/2$ sublevels even at 5 times the threshold energy. For H-like Xe^{53+} and Dy^{65+} ions, discrepancies become big, especially for high incident energy. Furthermore, for the high-Z U^{91+} ions, results with and without BI differ significantly even at rather lower incident energy. For example, at 2 times the threshold energy, the BI leads to a decrease in the cross sections by about 15% for the $M_f = -1/2$ sublevel and a increase by about 22% for the $M_f = -3/2$ sublevel compared to calculations without BI included.

For the $M_f = 1/2$ and $3/2$ sublevels, as shown in Figure 4, cross sections for excitation to the $M_f = 1/2$ sublevel remain significantly larger than those for to the $M_f = 3/2$ sublevel in all the H-like ions and at all incident energies. The differences between the $M_f = 1/2$ and $3/2$ magnetic sublevels cross sections decrease as the incident energy increases. These characters are quite similar with the same line for the EIE process studied by Reed and Chen [13] and Bostock et al. [14], and the RR process studied by Bettadj et al. [43], in which the $M_f = 1/2$ sublevel is preferentially populated in all of the H-like ions. The BI leads to a decrease in the $M_f = 1/2$ sublevel cross sections, while it make an increase in the $M_f = 3/2$ sublevel cross sections at all incident energies. This effect becomes more and more evident as the atomic number increases. For example, the effect of the BI on the $M_f = 3/2$ and $1/2$ sublevels is about 6% and 4% for H-like Fe^{25+} ions while about 65% and 32% for H-like U^{91+} ions at 5 times the threshold energy, respectively. Moreover, it is intersting to see that, for H-like U^{91+} ions, due to the BI effect, cross

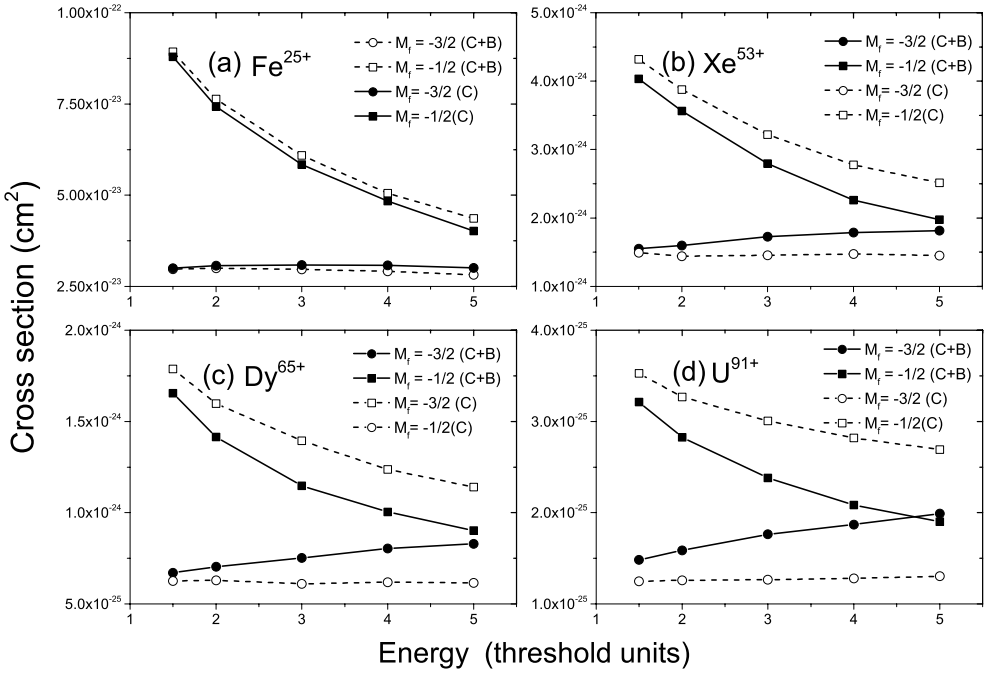

Fig. 3. The same as in Figure 2, but for $M_f = -1/2$ and $-3/2$ magnetic sublevels.

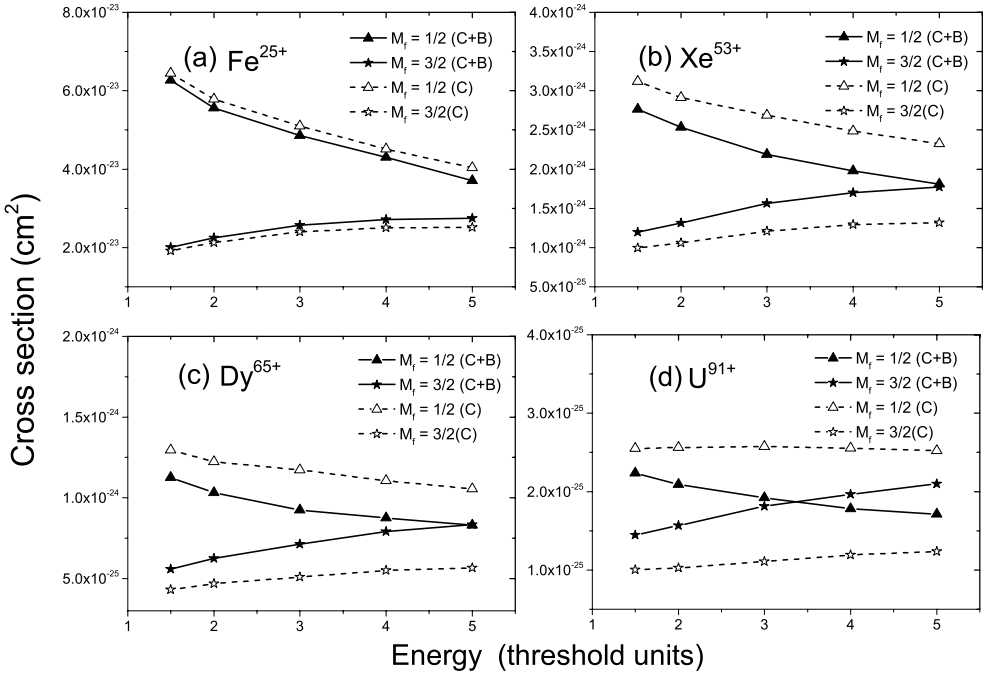

Fig. 4. The same as in Figure 2, but for $M_f = 1/2$ and $3/2$ magnetic sublevels.

section curves for the $M_f = -3/2$ and $-1/2$ sublevels and, the $M_f = 1/2$ and $3/2$ sublevels cross each other at about 4.7 and 3.4 times the threshold energy, respectively.

3.3 BI effects on the circular polarizations

Figure 5 shows the influences of the BI on the degrees of circular polarizations $P_c(\theta = 0)$ for the Lyman-α_1 line of H-like Fe^{25+}, Xe^{53+}, Dy^{65+}, and U^{91+} ions as functions of incident polarized electron energy in threshold units. In the calculations, we do not included the $E1$-$M2$ interference. It is can be found that the circular polarizations (absolute value) with and without the BI are monotonically decreasing with increasing incident energy and the curves do not intersect. For H-like Fe^{25+} and Xe^{53+} ions, two curves with and without the BI are close to each other for low energies (near threshold), with increasing energies,

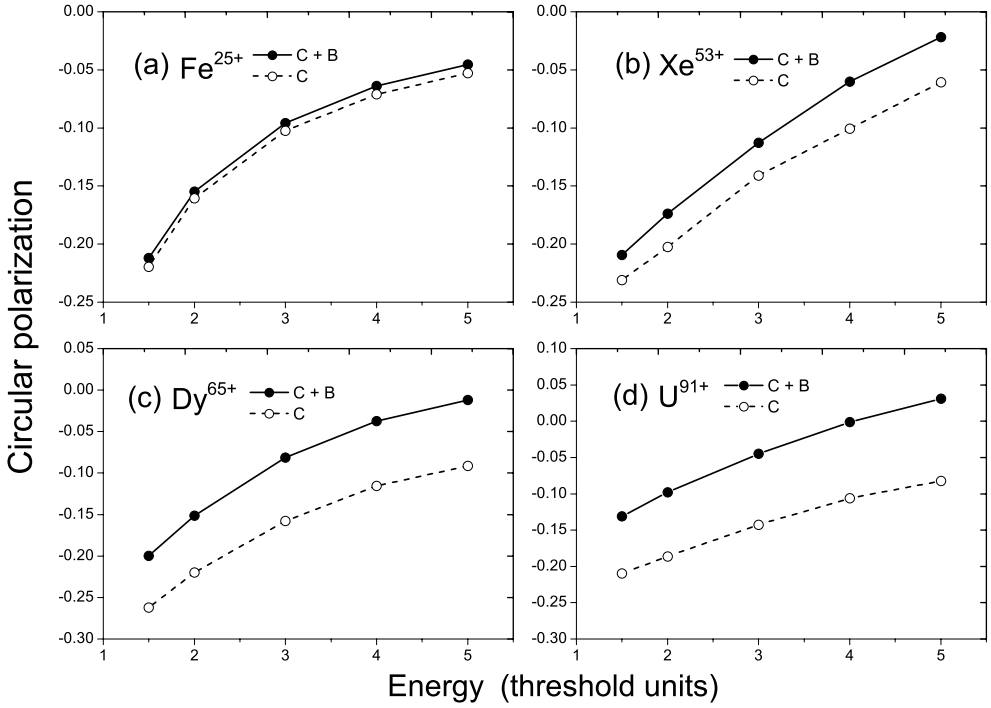

Fig. 5. Circular polarization $P_c(\theta = 0)$ for the Lyman-α_1 ($2p_{3/2} \rightarrow 1s_{1/2}$) transition line of H-like Fe^{25+}, Xe^{53+}, Dy^{65+}, and U^{91+} ions as functions of incident energy. C + B and C represent the values with and without inclusion of BI, respectively.

the differences become more noticeable. As expected, since relativistic effect is more dominant for high-Z elements, there is significant difference between the circular polarization with or without the BI for Dy^{65+} and U^{91+} ions. That is, the no BI result decreases less steeply with energy than the BI result and, the BI curve departs from the no BI curve at higher energies. For example, the BI leads to a decrease in the circular polarization by about 24% and 37% at 1.5 times the threshold energy, while about 86% and 135% at 5 times the threshold energy for H-like Dy^{65+} and U^{91+} ions, respectively.

Figure 6 shows the influences of the BI on the degree of circular polarization $P_c(\theta)$ for the Lyman-α_1 ($2p_{3/2} \rightarrow 1s_{1/2}$) transition line of H-like ions a function of the observation angle θ at four times the threshold energy. Obviously, in all ions, the maximum polarization (absolute value) occurs at $\theta = 0°/180°$. The differences between the angular distribution of the $P_c(\theta)$ with/without BI included are become more and more evident as the atomic number increases and as the θ tends to $0°/180°$.

To show the dependence of the circular polarization of X-ray radiation on the atomic number more clearly, in Figure 7, the circular polarizations $P_c(\theta = 0)$ with and without BI for the Lyman-α_1 radiation line at 4 times the threshold energy are displayed versus the atomic number. It is evident that the circular polarization (absolute value) decreases as the atomic number increases. However, with/without BI included, it decreases rapidly/slowly. The contribution of the BI to the circular polarizations for H-like Mo^{41+}, Xe^{53+}, Dy^{65+}, and U^{91+} ions is about 46%, 57%, 67%, and 98%, respectively.

3.4 Circular polarization including E1-M2 mixing

As mentioned, for the high-Z ions, the question of how multipole effects modify the circular polarization of X-ray radiation has not been considered before. To discuss the $E1$-$M2$ interference effects on the circular polarization of X-ray emission, in Table 2, we listed the pure $E1$ and $M2$ transition rates of Lyman-α_1 transition line for H-like Fe^{25+}, Xe^{53+}, Dy^{65+}, and U^{91+} ions, along with the existing theoretical values [33,44,45]. It is found that the ratios of A_{M2}/A_{E1} increase as the atomic number increases, which implies that the $M2$ radiative decay becomes more and more important for these high-Z ions. It is also found that the agreement with the different calculations is good in general for these transition rates. A discrepancy of <8% is quoted between other's results and the present calculations.

Figure 8 shows the influences of $E1$-$M2$ interference on the circular polarizations $P_c(\theta = 0)$ for the Lyman-α_1 transition line of H-like Fe^{25+}, Xe^{53+}, Dy^{65+}, and U^{91+} ions as functions of incident energy (threshold units). Here E1+M2 and E1 represent the values with and without inclusion of $E1$-$M2$ interference effects, respectively. In the calculations, we included the BI. As shown in Figure 8, both circular polarizations (absolute value) with and without the interference effects decrease monotonically with increasing incident energy. The $E1$-$M2$ interference may become important leading to considerable decreases in the circular polarization near the threshold, while these effects become less important as the incident energy increases. For example, the contributions of the $E1$-$M2$ interference effects to the circular polarization for H-like Fe^{25+}, Xe^{53+},

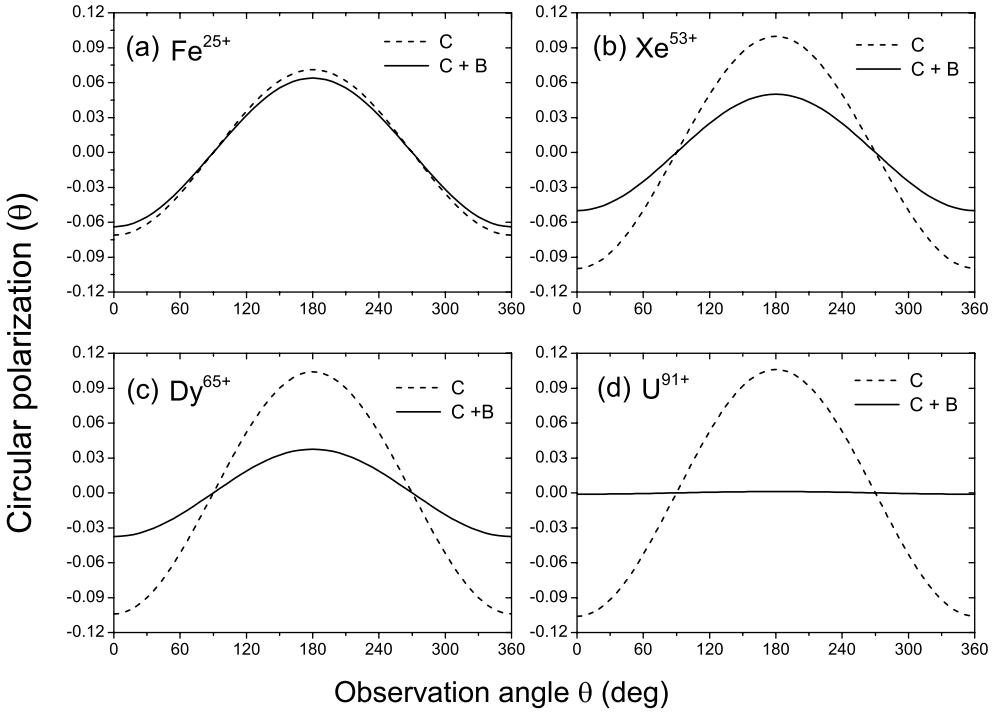

Fig. 6. Degree of circular polarization $P_c(\theta)$ for the Lyman-α_1 ($2p_{3/2} \rightarrow 1s_{1/2}$) transition line of H-like ions a function of the observation angle θ at four times the threshold energy. C + B and C represent the values with and without inclusion of BI, respectively.

Dy^{65+}, and U^{91+} ions are about 6%, 17%, 24%, and 42% at 1.5 times the threshold energy and, about 2.9%, 3.4%, 4%, and 18% at 5 times the threshold energy, respectively. Moreover, it is interesting to noted that, for H-like U^{91+} ions, two circular polarization curves with and without $E1$-$M2$ interference effects cross each other at about 4 times the threshold energy.

Finally, in Figure 9, we show the influence of the $E1$-$M2$ interference on the degree of circular polarization $P_c(\theta = 0)$ as a function of atomic number at 1.5 times the threshold energy for the Lyman-α_1 transition line of highly charged H-like ions. By inspecting Figure 9, one can clearly see that the $E1$-$M2$ interference effects decrease the circular polarization (absolute value) for H-like ions. Circular polarizations with $E1$ approximation/$E1$-$M2$ interference changes relatively slowly/rapidly as the atomic number increases [23]. These characteristics are different from the conclusions of the same radiation line but for the linear polarization emitted subsequent to the $2p_{3/2}$ population by the REC [29], EIE [23], and RR process [43].

Up now, we have studied the BI and radiation multipoles effects on the direct longitudinally-polarized EIE and de-excitation processes. It is hoped that the present results will stimulate interest in the unidirectional spin-polarized electrons collision experiments [36]. It is also hoped that some similar effects will be important during the positron impact ionization and the transversely polarized EIE processes. This may be an interesting topic for the future. For example, in the positron impact process, for the forward/back scattering, the paths of the electron and the positron are almost the same/different in the strong Coulomb field [46]. Moreover, apart from the direct excitation, the cascade and resonance excitation from higher lying shells may influence the cross sections and polarization in some case. These effects will be done in future works.

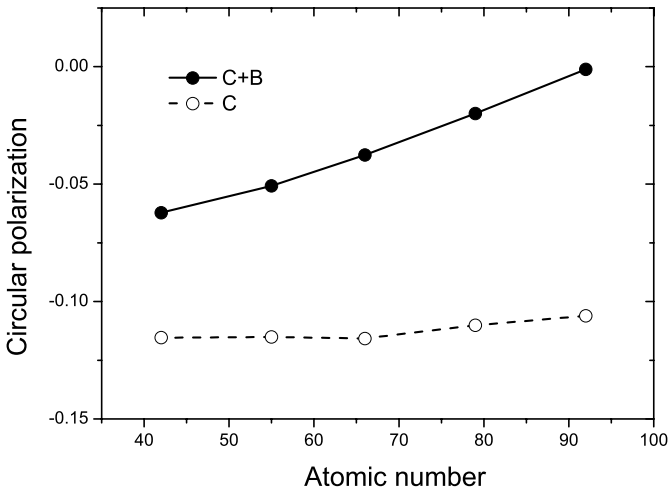

Fig. 7. Degree of circular polarization $P_c(\theta = 0)$ for the Lyman-α_1 ($2p_{3/2} \rightarrow 1s_{1/2}$) transition line of H-like ions a function of atomic number at four times the threshold energy. C + B and C represent the values with and without inclusion of BI, respectively.

Table 2. Comparison of the transition rates (s^{-1}) of the Lyman-α_1 line ($2p_{3/2} \rightarrow 1s_{1/2}$) for H-like ions between the present calculated results and the existing theoretical results. (B: Babushkin gauge, C: Coulomb gauge) $R[n]$ means $R \times 10^n$.

Ions	Type	Present	Others
Fe^{25+}	$E1$	2.84[14]^C, 2.84[14]^B	
	$M2$	9.89[9]	
Xe^{53+}	$E1$	5.11[15]^C, 5.13[15]^B	
	$M2$	3.55[12]	
Dy^{65+}	$E1$	1.09[16]^C, 1.12[16]^B	
	$M2$	1.81[13]	
U^{91+}	$E1$	3.69[16]^C, 3.93[16]^B	3.95[16][a], 3.92[16][b], 3.34[16][c]
	$M2$	2.80[14]	2.82[14][b]

[a]Reference [44], [b]reference [33], [c]reference [45]

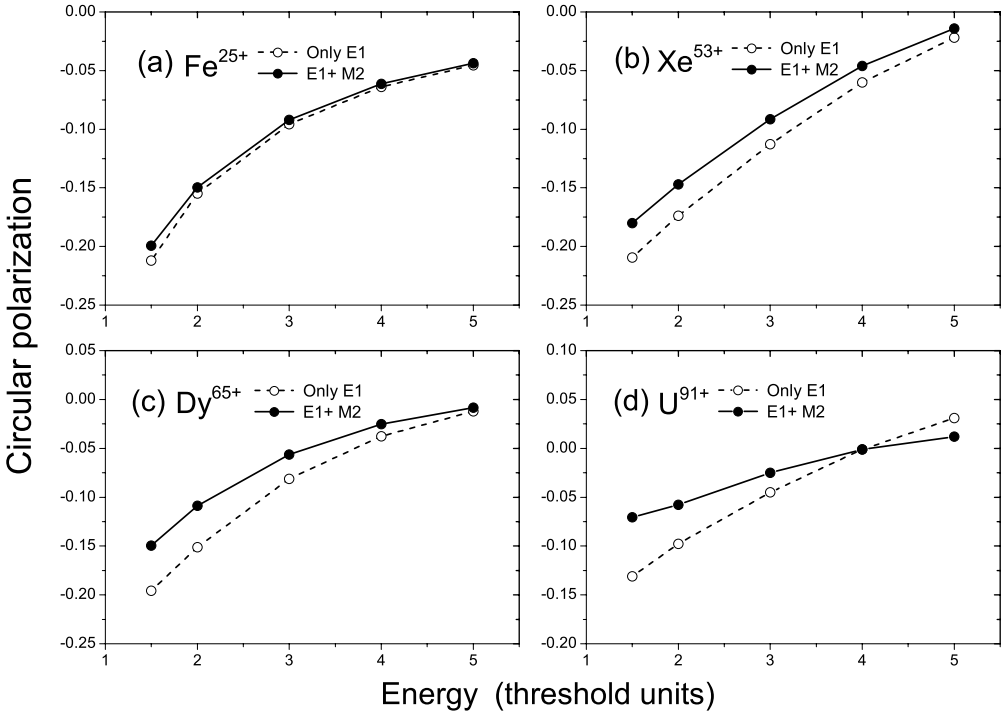

Fig. 8. Circular polarization $P_c(\theta = 0)$ for the Lyman-α_1 ($2p_{3/2} \rightarrow 1s_{1/2}$) transition line of H-like Fe^{25+}, Xe^{53+}, Dy^{65+}, and U^{91+} ions as functions of incident energy. E1 + M2 and E1 represent the values with and without inclusion of $E1$-$M2$ interference effects, respectively.

4 Conclusion

In summary, detailed calculations of the longitudinally-polarized EIE cross sections and the degree of circular polarizations of X-ray emission of the Lyman-α_1 ($2p_{3/2} \rightarrow 1s_{1/2}$) line for highly charged H-like Fe^{25+}, Xe^{53+}, Dy^{65+}, and U^{91+} ions are performed, including a detailed analysis of the influences of BI and radiation multipoles. It is found that the BI may leads to a dramatic change in the magnetic sublevels cross sections and circular polarizations of Lyman-α_1 ($2p_{3/2} \rightarrow 1s_{1/2}$) line radiation with a more pronounced effect at higher incident energies and/or atomic numbers. For example, for low-Z Fe^{25+} ions, BI effects on the cross sections and circular polarizations are small, they do not exceed 10% over the whole energy range considered, while for high-Z U^{91+} ions, the contributions of the BI to the circular polarizations are about 37% and 135% at 1.5 and 5 times the threshold energy, respectively. It is also found that, due to the $E1$-$M2$ interference effects, circular polarization $P_c(\theta = 0)$ (absolute value) decreases at a given incident energy, these features are more pronounced for higher atomic numbers. For example, the contributions of the $E1$-$M2$ interference effects to the circular polarizations of H-like Fe^{25+}, Xe^{53+}, Dy^{65+}, and U^{91+} ions are 6%, 17%, 24%, and 42% at about 1.5 times the threshold energy and 2.9%, 3.4%, 4%, and 18% at 5 times the threshold energy, respectively. The circular polarizations of the Lyman-α_1 line are exhibit a different behavior than the linear polarizations for the same transition line in the REC, EIE, and RR processes.

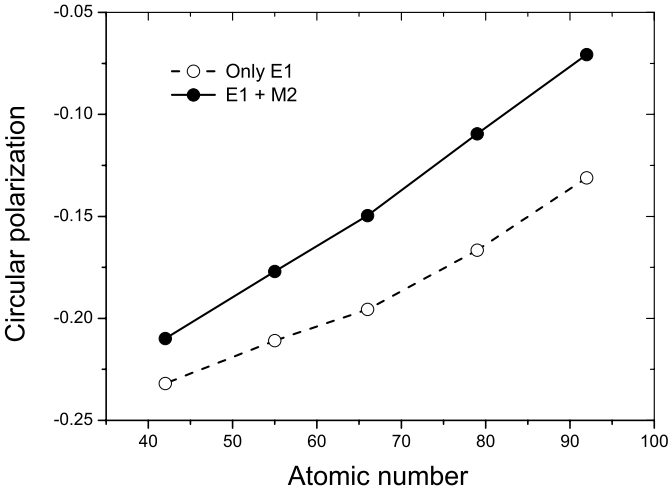

Fig. 9. Degree of circular polarization $P_c(\theta = 0)$ for the Lyman-α_1 ($2p_{3/2} \rightarrow 1s_{1/2}$) transition line of H-like ions as a function of atomic number at 1.5 times the threshold energy. E1+M2 and E1 represent the values with and without inclusion of $E1$-$M2$ interference effects, respectively.

One of the authors Z.B.C. would like to thank Professor C.Z. Dong (Northwest Normal University) for his kind help. This work was supported by the National Natural Science Foundation of China (Grant No. 11274382).

References

1. O. Matula, S. Fritzsche, F.J. Currell, A. Surzhykov, Phys. Rev. A **84**, 052723 (2011)
2. A. Gumberidze et al. Phys. Rev. Lett. **110**, 213201 (2013)
3. A. Surzhykov, S. Fritzsche, T. Stölker, Hyperfine Interact. **35**, 146 (2003)
4. Y.L. Shi, C.Z. Dong, X.Y. Ma, Z.W. Wu, L.Y. Xie, S. Fritzsche, Chin. Phys. Lett. **30**, 063401 (2013)
5. M.K. Inal, J. Dubau, Phys. Rev. A **47**, 4794 (1993)
6. M.K. Inal, J. Dubau, J. Phys. B **20**, 4221 (1987)
7. E. Takács, E.S. Meyer, J.D. Gillaspy, J.R. Roberts, C.T. Chantler, L.T. Hudson, R.D. Deslattes, C.M. Brown, J.M. Laming, J. Dubau, M.K. Inal, Phys. Rev. A **54**, 1342 (1996)
8. N. Nakamura, D. Kato, N. Miura, T. Nakahara, S. Ohtani, Phys. Rev. A **63**, 024501 (2001)
9. L. Sharma, A. Surzhykov, R. Srivastava, S. Fritzsche, Phys. Rev. A **83**, 062701 (2011)
10. Z.B. Chen, J.L. Zeng, C.Z. Dong, J. Phys. B **48**, 045202 (2015)
11. D.L. Robbins et al., Phys. Rev. A **74**, 022713 (2006)
12. P. Beiersdorfer, G. Brown, S. Utter, P. Neill, K.J. Reed, A.J. Smith, R.S. Thoe, Phys. Rev. A **60**, 4156 (1999)
13. K.J. Reed, M.H. Chen, Phys. Rev. A **48**, 3644 (1993)
14. C.J. Bostock, D.V. Fursa, I. Bray, Phys. Rev. A **80**, 052708 (2009)
15. C.J. Fontes, H.L. Zhang, D.H. Sampson, Phys. Rev. A **59**, 295 (1999)
16. Z.W. Wu, J. Jiang, C.Z. Dong, Phys. Rev. A **84**, 032713 (2011)
17. N. Nakamura, A.P. Kavanagh, H. Watanabe, H.A. Sakaue, Y. Li, D. Kato, F.J. Currell, S. Ohtani, Phys. Rev. Lett. **100**, 073203 (2008)
18. Z. Hu, X. Han, Y. Li, D. Kato, X. Tong, N. Nakamura, Phys. Rev. Lett. **108**, 073002 (2012)
19. S. Fritzsche, A. Surzhykov, T. Stölker, Phys. Rev. Lett. **103**, 113001 (2009)
20. R.E. Marrs, S.R. Elliott, D.A. Knapp, Phys. Rev. Lett. **72**, 4082 (1994)
21. C.J. Fontes, D.H. Sampson, H.L. Zhang, Phys. Rev. A **51**, R12 (1995)
22. S. Fritzsche, N.M. Kabachnik, A. Surzhykov, Phys. Rev. A **78**, 032703 (2008)
23. Z.B. Chen, C.Z. Dong, L.Y. Xie, J. Jiang, Phys. Rev. A **90**, 012703 (2014)
24. D. Bernhardt et al., Phys. Rev. A **83**, 020701(R) (2011)
25. J. Jiang, C.Z. Dong, L.Y. Xie, J.G. Wang, Phys. Rev. A **78**, 022709 (2008)
26. P. Amaro, F. Fratini, S. Fritzsche, P. Indelicato, J.P. Santos, A. Surzhykov, Phys. Rev. A **86**, 042509 (2012)
27. Z.W. Wu, C.Z. Dong, J. Jiang, Phys. Rev. A **86**, 022712 (2012)
28. T. Kai, S. Nakazaki, T. Kawamura, H. Nishimura, K. Mima, Phys. Rev. A **75**, 062710 (2007)
29. G. Weber et al. Phys. Rev. Lett. **105**, 243002 (2010)
30. A. Surzhykov, Y. Litvinov, T. Stöhlker, S. Fritzsche, Phys. Rev. A **87**, 052507 (2013)
31. L. Safari, P. Amaro, S. Fritzsche, J.P. Santos, S. Tashenov, F. Fratini, Phys. Rev. A **86**, 043405 (2012)
32. L. Safari, P. Amaro, S. Fritzsche, J.P. Santos, F. Fratini, Phys. Rev. A **90**, 014502 (2014)
33. A. Surzhykov, S. Fritzsche, A. Gumberidze, T. Stöhlker, Phys. Rev. Lett. **88**, 153001 (2002)
34. S. Fritzsche, A. Surzhykov, T. Stöhlker, Phys. Scr. **T144**, 014002 (2011)
35. A. Surzhykov, L. Sharma, T. Stöhlker, S. Fritzsche, J. Phys.: Conf. Ser. **212**, 012032 (2010)
36. R. Barday et al., J. Phys.: Conf. Ser. **298**, 012022 (2011)
37. M.K. Inal, H.L. Zhang, D.H. Sampson, Phys. Rev. A **46**, 2449 (1992)
38. M.K. Inal, D.H. Sampson, H.L. Zhang, J. Dubau, Phys. Scr **55**, 170 (1997)
39. M.K. Inal, H.L. Zhang, D.H. Sampson, C.J. Fontes, Phys. Rev. A **65**, 032727 (2002)
40. F.A. Parpia, C.F. Fischer, I.P. Grant, Comput. Phys. Commun. **94**, 249 (1996)
41. S. Fritzsche, H. Aksela, C.Z. Dong, S. Heinäsmäki, J.E. Sienkiewicz, Nucl. Instr. Meth. Phys. Res. B **205**, 93 (2003)
42. Z.B. Chen, C.Z. Dong, J. Jiang, Phys. Rev. A **90**, 022715 (2014)
43. L. Bettadj, M.K. Inal, M. Benmouna, J. Phys. B **47**, 105205 (2014)
44. V.G. Palchikov, Phys. Scr. **57**, 581 (1998)
45. S.N. Nahar, A.K. Pradhan, S. Lim, Can. J. Phys. **89**, 483 (2011)
46. V.A. Yerokhin, A. Surzhykov, R. Märtin, S. Tashenov, G. Weber, Phys. Rev. A **86**, 032708 (2012)